# Myelin development in visual scene-network tracts beyond late childhood: A multimethod neuroimaging study

Tobias W. Meissner[a,b], Erhan Genç[c], Burkhard Mädler[d], Sarah Weigelt[a]

[a] TU Dortmund University, Faculty of Rehabilitation Sciences, Department of Vision, Visual Impairments & Blindness, Emil-Figge-Str. 50, 44227 Dortmund, Germany

[b] Ruhr University Bochum, Faculty of Psychology, Universitätsstr. 150, 44801 Bochum, Germany

[c] Ruhr University Bochum, Faculty of Psychology, Institute for Cognitive Neuroscience, Department of Biopsychology, Universitätsstr. 150, 44801 Bochum, Germany

[d] Philips GmbH, Health Systems Department, Hamburg, Germany

**Corresponding author:** Tobias W. Meissner, tobias.meissner@rub.de, ORCHID ID: https://orcid.org/0000-0003-3972-5386

**Email of co-authors:** EG: erhan.genc@rub.de, BM: burkhard.maedler@philips.com, SW: sarah.weigelt@tu-dortmund.de

# Highlights

- Myelin in intrahemispheric scene-network tracts increases beyond late childhood
- Tracts connecting OPA and hippocampus, V1, and V2, also show prolonged myelination
- Diffusion tensor imaging parameters do not mirror myelin water fraction results

# Abstract

The visual scene-network—comprising the parahippocampal place area (PPA), retrosplenial cortex (RSC), and occipital place area (OPA)—shows a prolonged functional development. Structural development of white matter that underlies the scene-network has not been investigated—despite its potential influence on scene-network function. The key factor for white matter maturation is myelination. However, research on myelination using the gold standard method of post-mortem histology is scarce. *In vivo* alternatives diffusion tensor imaging (DTI) and myelin water imaging (MWI) so far report broad-scale findings that prohibit inferences concerning the scene-network. Here, we combine MWI, DTI tractography, and fMRI to investigate myelination in scene-network tracts in middle childhood, late childhood, and adulthood. We report increasing myelin from middle childhood to adulthood in lRSC-lOPA, rPPA-rRSC, and lPPA-lRSC tracts. Moreover, tracts connecting the OPA to the key input regions hippocampus, V1, and V2 showed myelin increases beyond late childhood. Our findings indicate that structural development coincides with functional development in the scene network, possibly enabling structure-function interactions.

# Keywords

white matter, maturation, connectivity, diffusion tensor imaging, scene recognition, high-level vision

# 1 Introduction

The human cortical visual system contains three high-level areas that preferentially respond to scenes compared to other stimuli, e.g. objects or faces: the parahippocampal place area (PPA, Epstein and Kanwisher, 1998), the retrosplenial cortex (RSC, O'Craven and Kanwisher, 2000), and the occipital place area (OPA, Grill-Spector, 2003; Hasson et al., 2003). This functional network is strongly involved in scene processing (e.g. Bettencourt and Xu, 2013; Dilks et al., 2011; Epstein et al., 2007a), but also in orientation and navigation (e.g. Epstein, 2008; Julian et al., 2016). The scene-network's components are already evident in middle childhood but at least for the PPA and the OPA there is evidence for a protracted development in terms of functional size and scene-selectivity beyond late childhood, possibly until adulthood (Chai et al., 2010; Golarai et al., 2007; Meissner et al., 2019b).

Despite this beginning understanding of the developmental trajectory of scene-network function between middle childhood and adulthood, the development of the white matter structure that underlies the scene-network has not received attention so far. However, white matter microstructure changes in corresponding brain areas were shown to be an underlying mechanism for specific cognitive development or differences, as has been shown for musical proficiency (Bengtsson et al., 2005), vocabulary development (Pujol et al., 2006), and many other cognitive abilities (for an overview, see Fields, 2008). Thus, maturational status of scene-network white matter structure might influence scene-network gray matter functional development, or vice versa (Fields, 2015; Zatorre et al., 2012).

Given that the PPA, RSC, and OPA contribute to the complex tasks of scene processing and navigation through (at least partially) distinct functional response properties (Baldassano et al., 2016; Epstein et al., 2007b; Epstein and Higgins, 2007; Hutchison et al., 2014; Vass and Epstein, 2013), mature, i.e. efficient transmission of signals between these areas is considered to be crucial for building an integrated perception for scenes. Signal transmission can be optimized through increasing speed, synchrony, or reliability—all of which are mediated by increases in axon myelination (Miller, 1994; Zatorre et al., 2012).

Measuring myelin accurately is only feasible in post-mortem histological studies. However, post mortem-studies are rare in general and most studies focus on newborns' and young infants' gray matter myelin content. In the only study investigating white matter myelin development beyond middle childhood based on histological observations, the authors report tract-specific maturation patterns featuring peak myelin growth rates within the first two years after birth as well as continued maturation up middle childhood (Yakovlev and Lecours, 1967). Evidence for development beyond childhood was limited to intracortical neuropil and association areas but should be regarded as rather anecdotal due to the low number of investigated tracts and specimens in that age group.

Due to the very limited availability of specimens for gold standard myelin assessment, the advance of diffusion tensor imaging (DTI), a non-invasive magnetic resonance imaging (MRI) method that has the potential to inform about myelin *in vivo*, was a milestone. DTI has been applied to probe developmental changes in white matter myelination extensively. However, most studies focused on major long fiber tracts, such as the internal capsule or the corticospinal tract, that can be readily identified (semi-) automatically using brain atlases (e.g. Lebel and Beaulieu, 2011; Mukherjee et al., 2001). As most long tracts are not directly involved in the visual scene-processing system and effects of age on white matter maturation were shown to be tract-specific (e.g. Rollins et al., 2010), the current literature is not informative on scene-network white matter development. Short-range tracts, which are crucial for relaying information in specialized functional networks over short distances, such as the scene-network, are understudied. The only relevant findings suggest ongoing myelination in temporal and parietal lobe short-range tracts (Oyefiade et al., 2018) or in white matter adjacent to dorsal and ventral visual stream cortical areas (Barnea-Goraly et al., 2005; Loenneker et al., 2011) and thus remain to unspecific for any inference on scene-network developmental trajectories.

DTI's sensitivity to myelin stems from its sensitivity to the diffusion of water because myelin reduces the inter-axonal space, increasing the anisotropy of water diffusion as a consequence (Feldman et al., 2010). However, several microstructural properties, such as axon diameter, axon packing density (Takahashi et al., 2002), axon membrane permeability (Ford et al., 1998), and fiber geometry (van Wedeen et al., 2005) affect DTI parameters, too. Therefore, deducing myelination or

maturational status from DTI parameters alone is challenging in most and speculative in some cases (Jones et al., 2013).

Myelin water imaging (MWI, MacKay et al., 1994), another MRI technique, is sensitive to myelin, highly reproducible (Meyers et al., 2009), and not affected by other microstructural changes, (Laule et al., 2008; Laule et al., 2006; Moore et al., 2000). Thus, it gives a more direct estimation of the status of myelination than interpretation of DTI parameters alone. Yet, MWI became available in pediatric research settings only recently, thanks to the implementation of parallel imaging (SENSE, Pruessmann et al., 1999) and advances in sequence design (Deoni et al., 2008; Prasloski et al., 2012) which both drastically sped up acquisition time.

A series of MWI studies investigated infants and young children and found steep increases of myelin from birth to age two and a moderate increase thereafter (e.g. Dean et al., 2015; Dean et al., 2014; Deoni et al., 2015; Deoni et al., 2012; Deoni et al., 2011). Recent findings indicate that while myelin does not seem to increase between middle and late childhood, a pronounced increase of myelin occurs in adolescence in major white matter tracts (Geeraert et al., 2018; Meissner et al., 2019a). However, scene-network specific data was not analyzed until now.

To complement recent findings regarding the functional development of scene-network regions PPA, RSC, and OPA (Meissner et al., 2019b), we combined MWI and DTI-based probabilistic tractography to probe the structural maturation, i.e. myelin water fraction (MWF), of white matter that underlies scene-network function in middle childhood (7-8 years), late childhood (11-12 years), and adulthood (19-24 years). Further, we tested if tracts that connect the scene-network with other key input areas, such as V1 and V2, or the hippocampus, which has been hypothesized to be part of the scene-network (Hodgetts et al., 2016), show increases myelination over time. In an extended analysis, we tested if DTI parameters mirror our MWI results.

# 2 Methods

## 2.1 Participants

We analyzed data of 18 children aged 7-8 (*M* = 7.56, *SD* = 0.51; 7 female; henceforth: 7-8yo), 13 children aged 11-12 (*M* = 11.23, *SD* = 0.44; 8 female; henceforth: 11-12yo) and 16 adults aged 19-24 (*M* = 20.69, *SD* = 1.14; 7 female) for this study. The original sample included one additional 7-8yo that was excluded due to severely impaired data quality in the DTI scan, one 7-8yo that did not complete the myelin water imaging scan, and one 11-12yo, in which our localizer failed to reveal any scene-selective ROIs. Participants took part in a larger study with several associated research questions. Thus, most participants‘ localizer data (see 2.2.2, Region of interest definition) was analyzed in a previous publication, which also holds detailed information on recruitment and compensation (Meissner et al., 2019b). All participants were healthy, had normal or corrected-to-normal vision, and had been born at term. No participant had past or current neurological or psychiatric conditions, or structural brain abnormalities.

## 2.2 Neuroimaging

All magnetic resonance images were acquired at the Neuroimaging Centre of the Research Department of Neuroscience at Ruhr University Bochum’s teaching hospital Bergmannsheil on a 3.0T Archieva scanner (Philips, Amsterdam, The Netherlands) using a 32-channel head coil. Acquisition of data reported in this manuscript were part of a longer protocol that included further functional scans. To reassure children and parents as well as to provide the possibility for low-threshold contact, children were accompanied by one of the experimenters in the scanner room throughout the entire procedure. Children who had not participated in an MRI study before were accustomed to the scanning environment, experimental procedure, and localizer task in a custom-built mock scanner at least one day prior to scanning. Participants were presented with short movie clips of a children’s TV program during the acquisition of structural MRI.

### 2.2.1 High-resolution anatomical imaging and cortical parcellation

To co-register magnetic resonance images from different sequence types (EPI, DTI, GRASE) as well as for gray-white matter segmentation and cortical parcellation, we acquired a T1-weighted high resolution anatomical scan of the whole head (MP-RAGE, TR = 8.10 ms, TE = 3.72 ms, flip angle = 8°, 220 slices, matrix size = 240 × 240, voxel size = 1 mm × 1 mm × 1 mm). We excluded non-brain parts of the head using FSL BET (Smith, 2002).

We used FreeSurfer (RRID: SCR_001847, version 6.0.0) for automated cortical parcellation and segmentation of the T1-weighted images. The details of the applied recon-all analysis pipeline have been described elsewhere (Dale et al., 1999; Fischl et al., 2004; Fischl et al., 2002; Fischl et al., 1999; Ségonne et al., 2004) and the procedure has been shown to be valid for all age groups in our study to the same extent (Ghosh et al., 2010).

To localize the primary and secondary visual area (V1 and V2) as well as the hippocampus, we used FreeSurfer's implemented probabilistic atlases (Fischl et al., 2008). We converted V1, V2, and hippocampus FreeSurfer surface labels to ROI masks in FSL anatomical T1 space using FreeSurfer's bbregister and mri_label2vol commands. Next, we registered V1, V2, and hippocampus masks to DTI space using FSL FLIRT (FMRIB's Linear Image Registration Tool, Greve and Fischl, 2009; Jenkinson et al., 2002; Jenkinson and Smith, 2001) for probabilistic tractography (Figure 1, top, middle).

### 2.2.2 Region of interest definition

To define scene-selective regions of interest (ROIs), we obtained functional MRI during a four-run scene localizer block design experiment that included scenes, objects, and a rest condition using a blood oxygen level dependent (BOLD) sensitive T2-weighted sequence across 33 slices (TR = 2000 ms, TE = 30 ms, flip angle = 90°, FOV = 240 mm × 240 mm, voxel size = 3 mm × 3 mm × 3 mm, slice gap = 0.4 mm). Details of the scene localizer experimental design are reported elsewhere (Meissner et al., 2019b).

We used FSL FEAT (FMRIB's Software Library, version 5.0.11, RRID: SCR_002823, Jenkinson et al., 2012; FMRI Expert Analysis Tool, version 6.0.0, Woolrich et al., 2001) for preprocessing and statistical analysis of functional MRI localizer data. Preprocessing of functional data included brain extraction, slice time correction, motion correction, high-pass temporal filtering (cutoff: 91 s) and registration to the T1 anatomical image for each run in a first-level analysis. First-level statistical results were then entered into a mixed-effects second-level analysis (FLAME 1 option;

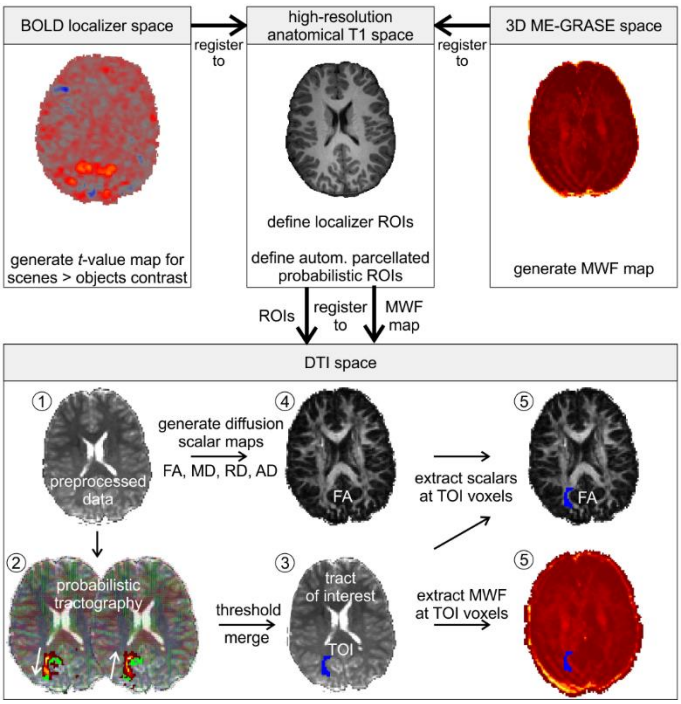


*Figure 1: Analysis pipeline overview. The anatomical image in T1 space was used as a common intermediate registration template and connecting link between DTI space and non-diffusion spaces, i.e. BOLD and GRASE space. Numbers in circles indicate the order of analysis steps in DTI space. green = seed and target ROI (here: rRSC & rOPA) for probabilistic tractography, heatmap arch = result for probabilistic tractography in which brighter colors indicate more samples crossing that voxel, blue = merged and thresholded TOI mask.*

Woolrich et al., 2004), yielding statistical *t*-value maps for the scene > object contrast for each participant

To define ROIs, we registered each participant's *t*-value maps to her/his anatomical T1 image using sinc interpolation with FSL FLIRT (Figure 1, top, left). Using FSLeyes (version 0.22.6, McCarthy, 2018), we manually defined subject-specific PPA, RSC, and OPA in each hemisphere at plausible locations (Figure 1, top, middle; for exemplary ROIs, see Figure 2a). For the PPA and RSC, we included contiguous voxels whose scenes > objects contrast exceeded the *t*-value of 5.75. For the OPA, we chose a more liberal threshold of $t > 4$, because the OPA can rarely be detected at the same threshold as the PPA and RSC (without melting PPA and RSC at liberal thresholds or not detecting the OPA a conservative thresholds; cf. Meissner et al., 2019b).

For all ROIs, this approach yielded in high detection rates that did not differ between age groups as determined using Fisher's exact test (S1 Table). One 11-12yo was excluded from subsequent analyses, because activations for the scenes > objects contrast did not exceed the set thresholds. We registered each ROI from anatomical T1 space to native DTI space using nearest neighbor interpolation with FSL FLIRT. For six ROIs, interpolation to the target space using the nearest neighbor algorithm failed. To still include these ROIs in the analysis, we applied a trilinear interpolation approach, followed by binary-coding the resulting continuous ROI-map at its median value.

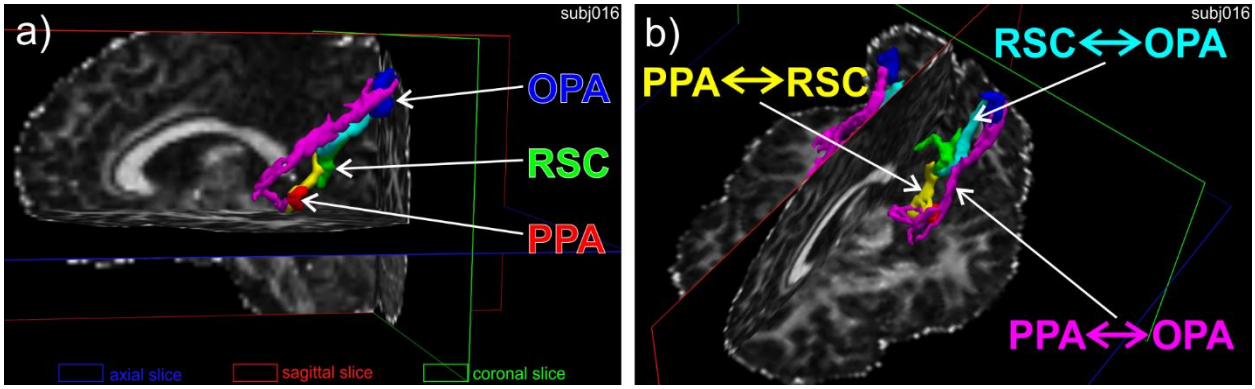


*Figure 2: Scene-selective areas (a) and fiber tracts (b) for an exemplary 7-8yo participant. Areas and tracts are reconstructed in native 3D DTI space on top of a FA map. Areas, tracts, and FA map are smoothed for better visualization. Tracts are displayed in uniform color for easier identification; for an example of a tract probability (heat-)map, see Figure 3, bottom, left.*

### 2.2.3 Diffusion weighted imaging

For fiber tracking and diffusion parameter analysis, a diffusion-weighted single-shot spin-echo EPI sequence along 33 isotropically distributed directions using a b-value of 1000 s/mm$^2$ (TR = 7234 ms, TE = 89 ms, flip angle = 90°, 60 slices, matrix size = 128 × 128, voxel size = 2 × 2 × 2 mm) was obtained. Prior to this sequence, one reference image was acquired without diffusion weighting (b = 0 s/mm$^2$). For analysis of diffusion weighted data, we used FSL's FDT (FMRIB's Diffusion Toolbox). Preprocessing of DTI data included eddy current and motion artefact correction using FSL eddy_correct, diffusion gradient vectors reorientation to match the correction-induced rotations, as well as brain extraction (Figure 1, bottom, #1).

We performed probabilistic tractography on our data in native diffusion space using FSL BEDPOSTX and PROBTRACKX (Behrens et al., 2007; Behrens et al., 2003) with default settings, but 25,000 tract-following streamlines originating from each seed mask voxel (Figure 1, bottom, #2). For each participant, fiber tracking was done for 24 intrahemispheric tracts. In turn, each of the six scene selective ROIs—as defined by our localizer (see 2.2.2, Region of interest definition)—was set as the seed mask. For each seed mask, i.e. for each scene selective ROI, five ipsilateral target masks were set: 1-2) the two other scene ROIs, 3) the hippocampus, 4) V1, and 5) V2 (Figure 3). For these 24 seed-target pairs, probabilistic tractography was done in both directions. That is, after the initial seed-to-target tracking was done, a target-to-seed tracking estimated the same tract in reverse direction (cf. Genç et al., 2011). For both directions, target masks were also set as waypoint and termination masks to ensure that only tracts would be retained that entered the target mask and that did not project onto other areas. Our rationale for employing this dual-direction approach was to control for any direction specific biases in probabilistic tractography, avoiding under- or overrepresentation of tract size or detectability. We refrained from interhemispheric tracking, as DTI and MWI parameters from these tracts would be masked by a major share of general corpus callosum development adding little—if any—insight into scene-network specific development (for corpus callosum development, see Meissner et al., 2019a).

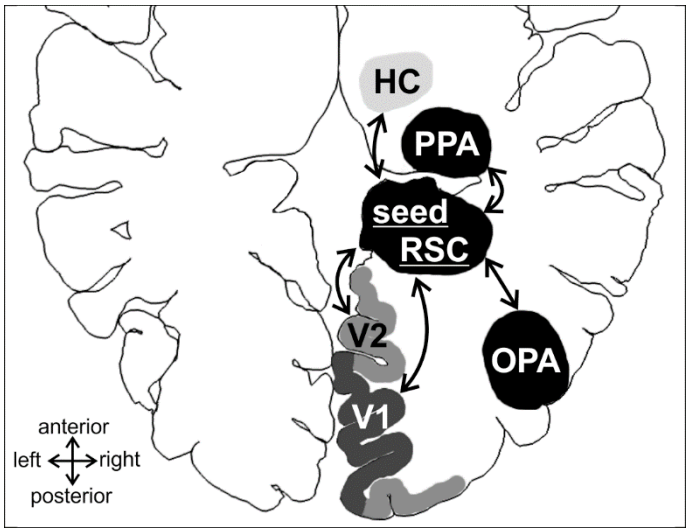


*Figure 3: Schematic exemplary seed region (rRSC) with target regions and tract connections. For each scene selective ROI, fiber tracking was done with the ipsilateral V1, V2, hippocampus (HC), and the other two ipsilateral scene selective ROIs (here: PPA and OPA). Note that in order to show all seed and target regions in one comprehensive display, this is a schematic drawing that does not reflect the appropriate absolute or relational position and size of target and seed regions.*

For each voxel, the resulting probability maps indicate how many of the streamlines that successfully connected seed-to-target crossed this voxel. However, these probability maps include low-probability voxels that are likely to be spurious connections. To remove these spurious connections, we threshold individual tract maps at 20% of their robust maximum (99th percentile) value (cf. Koldewyn et al., 2014) and then merged seed-to-target and target-to-seed tracts using a logical *and*-condition (Figure 1, bottom, #3; for exemplary tracts, see Figure 2b). Like other thresholding approaches, this accounts for systematically different ROI sizes. Moreover, in contrast to thresholding based on the number of initiated or successful streamlines, our approach provides a better interpretability, as the number of initiated or successful streamlines offers little insight into the actual probability map value distribution.

To evaluate white matter microstructural integrity in fiber tracts of interest, we fit diffusion tensors, modelled by three pairs of eigenvectors ($\varepsilon_1, \varepsilon_2, \varepsilon_3$) and eigenvalues ($\lambda_1, \lambda_2, \lambda_3$) that describe the direction and magnitude of water diffusion along three orthogonal axes, to each voxel of our preprocessed DTI data using FSL DTIFIT. We then calculated axial, radial and mean diffusivity (AD = $\lambda_1$, RD = $(\lambda_1 + \lambda_2)/2$, MD = $(\lambda_1 + \lambda_2 + \lambda_3)/3$), as well as fractional anisotropy (FA = $\sqrt{3/2} \times \sqrt{(\lambda_1 - \mathrm{MD})^2 + (\lambda_2 - \mathrm{MD})^2 + (\lambda_3 - \mathrm{MD})^2} / \sqrt{\lambda_1^2 + \lambda_2^2 + \lambda_3^2}$) as diffusion parameters of

interest (Figure 1, bottom, #4). Weighted DTI metric values for each tract were obtained that considered each voxel's DTI metric value and tract probability (voxel weight: number of streamlines crossing through a voxel in relation to the sum across all voxels, Figure 1, bottom, #5).

#### 2.2.4 Myelin water imaging

To examine the myelination state of white matter tracts, a 3D multi-echo (ME) gradient spin echo (GRASE) sequence with refocusing sweep angle was acquired (TR = 800 ms; TE = 10 - 320 ms, 32 echoes in steps of 10 ms, partial Fourier acquisition in both phase encoding directions, parallel imaging SENSE = 2.0, flip angle = 90°, 60 slices, matrix size = 112 × 112, voxel size = 2 × 2 × 2 mm, acquisition duration = 7.25 min). Parameter maps estimating the fraction of water molecules located between myelin layers—the myelin water fraction (MWF, MacKay et al., 1994 )—for each voxel were created as described elsewhere (Prasloski et al., 2012). MWF maps were then registered to native DTI space using FSL FLIRT (Figure 1, top, right and middle). Here, for high-accuracy transformations, we employed a two-step procedure. First, we registered the TE = 10 ms of the GRASE sequence to anatomical T1 space using trilinear transformation. The resulting transformation matrix was then used to register the MWF map to anatomical T1 space using sinc interpolation. Second, we registered the T1 anatomy to the b=0 DTI image using trilinear transformation. The resulting transformation matrix was then used to register the MWF map from anatomical T1 space to DTI space using sinc interpolation. As for DTI parameters, weighted mean MWF values for each tract were obtained that considered each voxel's MWF value and tract probability (Figure 1, bottom, #5).

### 2.3 Neuroimaging data quality control

We screened preprocessed 4D DTI data and FA maps for visible artefacts that were not corrected by the preprocessing steps and excluded one 7-8yo participant from subsequent analyses. Further, to control for possible age group differences in DTI data quality, we quantified two registration-based and two intensity-based data quality measures implemented in the FreeSurfer TRACULA toolbox (Yendiki et al., 2011). For the registration-based measures, mean volume-to-volume translation and rotation parameters were obtained from affine registration matrices of each volume to the first (b=0) volume. This was to capture global, slow between-volume motion. Our analysis of variance (ANOVA) on both translation and rotation parameters did not reveal any

significant between-group differences (Figure 4; rotation: $F(2,44) = 1.52$, $p = .230$, $\eta^2 = .065$ translation: $F(2,44) = 2.27$, $p = .115$, $\eta^2 = .094$)

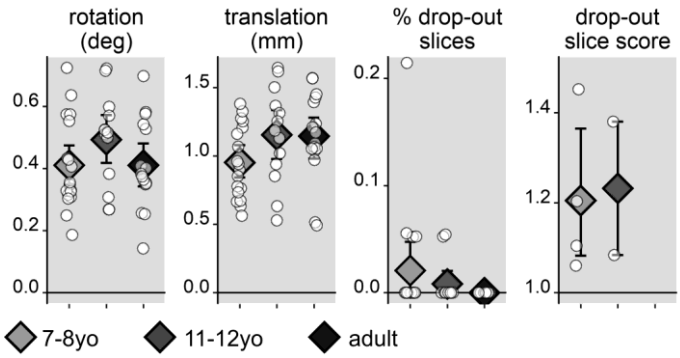


*Figure 4: Between-group data quality comparison after matching for the percentage of drop-out slices. Light gray = 7-8-year-old children, medium gray = 11-12-year-old children, dark gray = adults. White circles = individual data points. Gray diamonds = group mean. Error bars show 95% confidence intervals for the mean.*

For the intensity-based measures, we calculated a signal intensity drop-out score for each slice in each volume in reference to the corresponding slice in the b=0 volume as proposed by Benner et al. (2011). This was to capture the effect of rapid within-volume motion (note: TR = 7234 ms). We then quantified the percentage of slices with suspect signal drop-out across the scan—indicated by a score greater than 1—as well as the average signal drop-out severity for those "bad" slices. Four 7-8yo, two 11-12yo, but no adults displayed any slices with strong signal dropout (Figure 4). In participants with signal dropout, we observed a maximum portion for "bad" slices of 0.21 %. Due to the low number of participants with signal dropout, and no signal dropout in the adult group (i.e. no variance) any ANOVA-based group comparison for the drop-out slice score or percentage of drop-out slices would lack validity. Thus, we employed Fisher's exact test and found that the number of participants with any signal-dropout did not differ between age groups ($\chi^2(2) = 3.87$, $p = .152$).

As the 3D signal acquisition method of the GRASE sequence is not volume-based, affine registration matrices and corresponding motion estimates, like for functional MRI or DTI cannot be computed for 3D ME-GRASE data. However, we visually screened all raw GRASE images as well as MWF maps for motion artefacts but found none.

## 2.4 Experimental design, statistical analysis

Our study investigated the effect of the between-subject factor age group (with three levels) on the outcome variables MWF, FA, MD, RD, and AD for six scene selective fiber tracts. In an

exploratory analysis, further tracts were tested between all six scene selective ROIs and the V1, V2, and HC, respectively. To test for differences between age groups, we employed analysis of variances (ANOVAs) for each fiber tract independently. To correct for multiple comparison, the default significance threshold of $\alpha = .05$ was Bonferroni-corrected for 6 tracts to $\alpha = .0083$. To improve the usability of our results for colleagues whose research interest focuses on one or a particular region or tract of interest only, we also report age group effects that reached the uncorrected significance threshold of $\alpha = .05$ in a second step. Statistical data analysis was performed using R (version 3.2.2, RRID: SCR_001905, R Core Team, 2015) in RStudio (version 0.99.491; RRID: SCR_000432).

# 3 Results

This study combined myelin water imaging with a functional MRI scene localizer and DTI-based tractography to determine the degree of myelination in white matter tracts underlying the

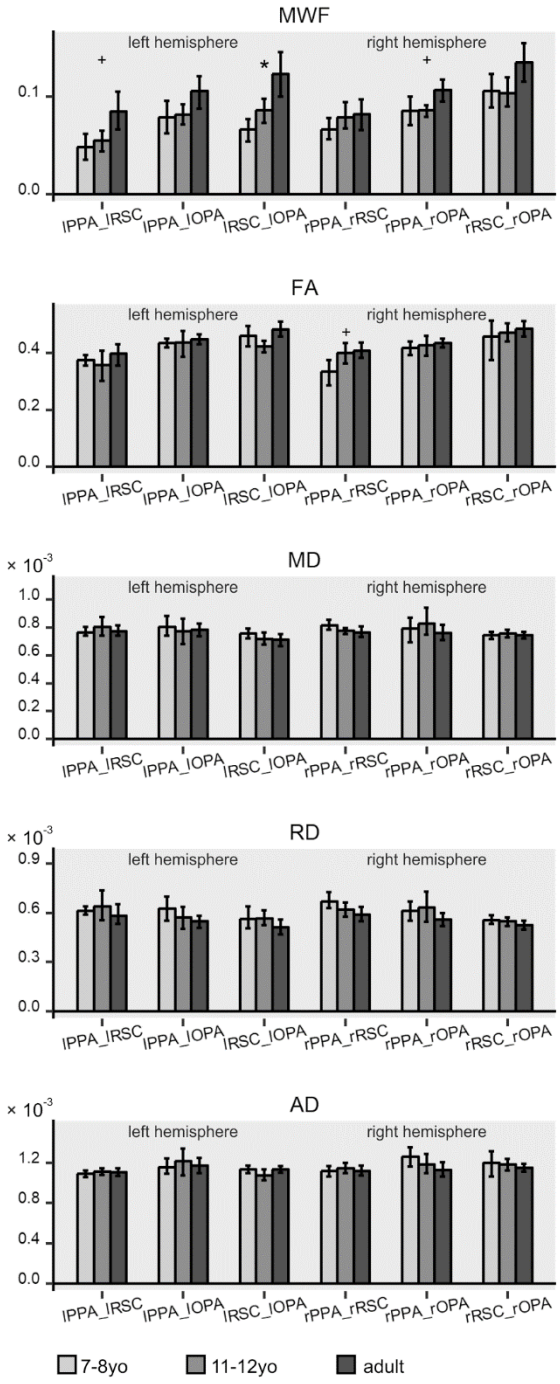


*Figure 5: Myelin water fraction (MWF) and DTI parameters for intrahemispheric connections between scene-network areas. Light gray = 7-8-year-old children, medium gray = 11-12-year-old children, dark gray = adults. Error bars show 95% confidence intervals for the mean. Asterix and plus signs indicate significance with Bonferroni correction (α = .0083) and without correction for multiple comparisons (α = .05), respectively.*

cortical scene-network in three age groups. We examined possible differences in myelin water fraction between eighteen 7-8yo, thirteen 11-12yo, and sixteen adults to identify if the scene-network's white matter structural connectivity follows a similar or divergent pattern in reference to scene-network's functional development. Further, we investigated connections between the scene-network and key input areas, such as V1 and V2, or the hippocampus. In an extended analysis, we tested if DTI parameters showed the same pattern as MWF.

## 3.1 Myelin water imaging

Regarding within-scene-network tracts, the MWF in fibers connecting lRSC and lOPA increased with age ($F(2,24) = 6.61$, $p = .0051$, $\eta^2 = .355$, Figure 5). We observed further increases, albeit only significant without Bonferroni correction for the lPPA-lRSC tract ($F(2,29) = 4.48$, $p = .0201$, $\eta^2 = .236$) and the rPPA-rOPA tract ($F(2,26) = 3.82$, $p = .0352$, $\eta^2 = .227$).

For connections between the HC and scene-network areas, we found increasing MWF with age in tracts connecting to the lOPA ($F(2,36) = 8.20$, $p = .0012$, $\eta^2 = .313$). MWF also increased in the rOPA, albeit only significant without Bonferroni correction ($F(2,35) = 4.77$, $p = .0147$, $\eta^2 = .214$, Figure 6, top left).

V1-scene-network connections showed increasing MWF with age in connections to the lOPA ($F(2,32) = 6.45$, $p = .0044$, $\eta^2 = .287$, Figure 6, top middle). We observed further increases that did not survive Bonferroni-correction for connections to the rOPA ($F(2,33) = 5.04$, $p = .0123$, $\eta^2 = .234$) and rRSC ($F(2,41) = 3.32$, $p = .0460$, $\eta^2 = .140$).

V2-scene-network connections showed increasing MWF with age in connections to the lOPA ($F(2,36) = 5.54$, $p = .0080$, $\eta^2 = .235$, Figure 6, top right). We observed further increases that did not survive Bonferroni-correction for connections to the lOPA ($F(2,35) = 3.97$, $p = .0279$, $\eta^2 = .185$) and lRSC ($F(2,38) = 4.07$, $p = .0251$, $\eta^2 = .176$).

## 3.2 Extended analysis of DTI parameters

Regarding within-scene-network tracts, the age group differences observed for MWF was not mirrored in DTI parameters. For FA, we found increasing MWF with age in the rPPA-rRSC tract, but

statistical significance did not meet our Bonferroni-correction criterion ($F(2,35) = 4.35$, $p = .0205$, $\eta^2 = .199$, Figure 5, second row). No other tract showed age effects for FA. Concerning the other DTI parameters—MD, RD, and AD—we did not find any tracts with age group differences (Figure 5, third, fourth, and fifth row).

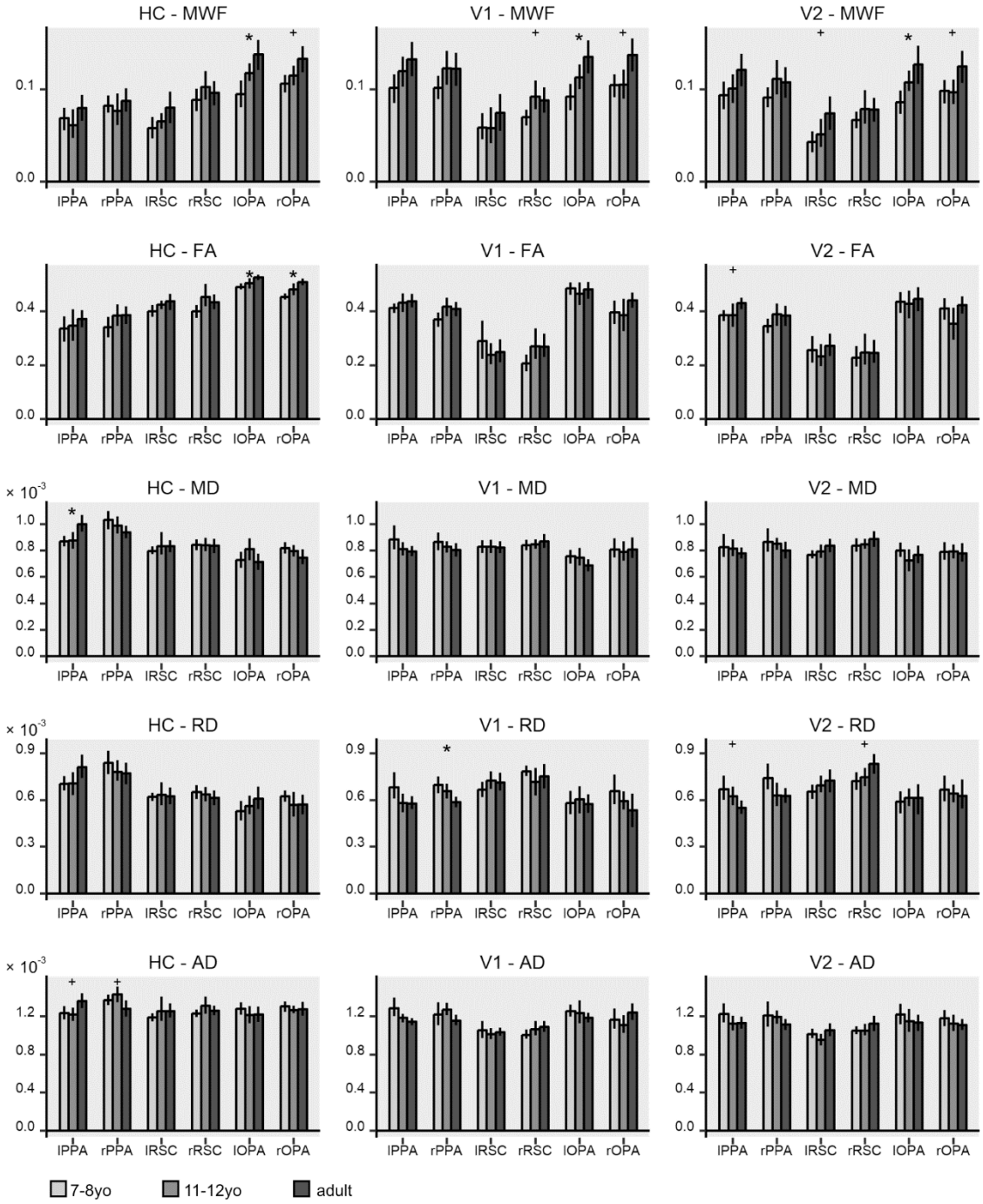


*Figure 6: Myelin water fraction (MWF) and DTI parameters for connections between scene-network areas and the hippocampus (HC, left), primary visual area (V1, middle), and secondary visual area (V2, right). Light gray = 7-8-year-old children, medium gray = 11-12-year-old children, dark gray = adults. Error bars show 95% confidence intervals for the mean. Asterix and plus signs indicate significance with Bonferroni correction (α = .0083) and without correction for multiple comparisons (α = .05), respectively*

HC-scene-network connections showed a similar pattern for FA as for MWF. Tracts from the HC to the lOPA and rOPA showed increasing FA with age (lOPA: $F(2,36) = 6.73$, $p = .0033$, $\eta^2 = .272$; rOPA: $F(2,35) = 11.49$, $p = .0001$, $\eta^2 = .396$, Figure 6, left, second row). However, other DTI parameters did not mirror MWF findings: MD showed an increase in HC-lPPA connections with age ($F(2,40) = 6.38$, $p = .0039$, $\eta^2 = .242$, Figure 6, left, third row), but not in other tracts. RD did not reveal differences between age groups in HC-connecting tracts. Concerning AD, tracts connecting the HC and the PPA showed age group differences, albeit increasing values for the left and decreasing values for the right hemisphere and not surviving Bonferroni-correction in either hemisphere (lPPA: $F(2,40) = 3.88$, $p = .0289$, $\eta^2 = .162$, rPPA: $F(2,40) = 3.42$, $p = .0426$, $\eta^2 = .146$, Figure 6, left, last row).

For V1-scene-network connections, the only age group differences in DTI parameters was found in the V1-rPPA tract as an RD decrease ($F(2,40) = 6.21$, $p = .0045$, $\eta^2 = .237$, Figure 6, middle, fourth row).

In V2-scene-network connections, DTI parameters did not exhibit age group differences that survived Bonferroni correction. However, uncorrected effects were evident in V2-lPPA tract for increasing FA ($F(2,40) = 3.32$, $p = .0465$, $\eta^2 = .142$) and decreasing RD ($F(2,40) = 3.53$, $p = .0389$, $\eta^2 = .150$) and in the V2-rRSC tracts for increasing RD ($F(2,41) = 3.57$, $p = .0372$, $\eta^2 = .148$).

## 3.3 Control analyses

To control for the possibility that any of the observed age effects were confounded by age-related tract volume differences, we compared tract volume between age groups using ANOVAs and found differences in lHC-lPPA, rHC-rPPA, and rHC-rOPA tracts, but not in any other tracts (lHC-lPPA: $F(2,40) = 6.27$, $p = .0043$, $\eta^2 = .239$; rHC-rPPA: $F(2,40) = 7.56$, $p = .0016$, $\eta^2 = .274$; rHC-rOPA: $F(2,40) = 6.10$, $p = .0054$, $\eta^2 = .258$). Thus, while FA effects in rHC-rOPA might stem from tract size differences between age groups, for all other tracts, volume seems an unlikely bias.

# 4 Discussion

Myelin emergence and further maturation is a crucial step in brain development (Flechsig, 1920). While myelin development trajectories for white matter beyond late childhood are still unclear, it is established that the rate of change and the point at which an adult level is reached is region specific (Yakovlev and Lecours, 1967). Further, myelin maturation was shown to interact with functional organization and behavior (e.g. Bengtsson et al., 2005; Yeatman et al., 2012). Here, we compared MWF in white matter tracts underlying the visual scene-network between 7-8yo, 11-12yo and adults. We found increasing MWF in lRSC-lOPA, rPPA-rRSC, and lPPA-lRSC tracts. Moreover, myelin increased in connections from the OPA to the key input regions hippocampus, V1, and V2, as well as in rRSC-V1 and lRSC-V2 connections.

## 4.1 Connections between scene network areas

These findings provide evidence for a protracted development of white matter tracts that connect the scene-network regions PPA, RSC, and OPA. While age effects were only significant after Bonferroni correction in the lRSC-lOPA tract, effect sizes for lPPA-lRSC and rPPA-rRSC tracts were medium-to-large. Thus, we are confident that a higher power in terms of more participants would have rendered these effects significant with Bonferroni correction, too. The three tracts that did not even pass the $\alpha = .05$ significance threshold show increasing mean MWF with age on a descriptive level. Altogether, this suggests an almost general increase in scene network tracts with some tracts displaying more pronounced age effects than others.

This pattern would suggest that scene network tracts' developmental trajectory resembles that of major long white matter tracts. Recent findings indicate that myelin in a majority of major white matter tracts increases from childhood into young adulthood (Meissner et al., 2019a). In this study, major tracts that may partly subserve scene network connecting tracts—the inferior longitudinal fasciculus, and the cingulum angular bundle—showed moderate myelin increases from middle childhood to adulthood. Moreover, this pattern suggests a resemblance to cortical gray matter myelin content development, which displays development across late adolescence and up to early adulthood, too (Carey et al., 2018; Grydeland et al., 2013; Miller et al., 2012; Shafee et al., 2015).

Integrating our results with recent findings of functional cortical development in scene selective areas during and beyond childhood (Chai et al., 2010; Golarai et al., 2007; Meissner et al., 2019b) opens up the possibility of structure-function interactions, i.e. influences of structural development on functional development, or vice versa. However, while previous studies established that the RSC is adult-like in middle childhood already (Jiang et al., 2014; Meissner et al., 2019b), tracts connecting the RSC to the PPA and the OPA in the left hemisphere displayed development nonetheless. Either, this could mean that if structure-function interactions exist, they do not need the involvement, i.e. development, of both cortical ends of a tract. Or, this could mean that no interactions exist, i.e. structural and functional development is independent. As cortical structure, function, and associated cognitive abilities have been associated with white matter structural development (Fields, 2008; Gomez et al., 2017), we speculate that a completely independent development of structure and function is unlikely.

## 4.2 Connections between the scene network, hippocampus, V1, and V2

Connections from HC, V1, and V1 to OPA, especially in the left hemisphere indicate increasing myelination from middle childhood to adulthood. Interestingly, functional cluster size as well as scene selectivity in bilateral OPA was shown to increase along the same trajectory (Meissner et al., 2019b). As for within-scene network connections, to speculate, functional OPA development could be driven by maturing connections to input/output areas. Or, vice, versa, the maturation of OPA-associated fibers could be a case of activity dependent myelination (Fields, 2008). Connections from rV1 to rRSC and from lV2 to lRSC showed moderate effect sizes but significance did not survive Bonferroni correction. The inconsistency of hemisphere and visual area hierarchy makes this finding difficult to interpret. Possibly, the observed effects are residuals of an activity-dependent myelination that started following the completion of functional RSC maturation.

## 4.3 Diffusion tensor imaging interpretation

None of the investigated DTI parameters (FA, MD, RD, AD), mirrored any MWI findings except for FA age effects in connections between the scene network and the hippocampus, where FA increases with age in lHC-lOPA and rHC-rOPA tracts (the latter might be confounded by age group differences in tract volume).

This generally missing correspondence might be explained by the fact that fiber geometry has a particularly high influence on DTI parameters in small tracts—like connections between scene-network areas. This is due to a higher probability that two tracts with diverging principal diffusion directions cross, branch, or merge within one voxel (Feldman et al., 2010). Thus, especially in small tracts, the use of DTI parameters as a proxy for myelin is problematic and might not reflect myelination but rather other microstructural changes (Moura et al., 2016). For example, a recent study that investigated major large tracts found a comparatively higher correspondence between DTI and MWF effects (Meissner et al., 2019a).

## 4.4 Outlook

Here, we investigated the development of myelin in white matter tracts subserving the cortical visual scene network for the first time. We established that myelin seems to increase in several within-scene network tracts as well as in connections to crucial input regions. These results are exciting in so far as they demonstrate that the protracted scene network development between childhood is not limited to functional changes, but also includes maturation of underlying structures that are not directly part of the cortical network. We believe that our study opens up two further directions going forward. First, our cross-sectional study paves the way for large-scale longitudinal studies with short time intervals over an extended period of time and a high number of participants that combine behavioral testing, fMRI, DTI-tractography, and MWI, which could tap into the important question of structure-function-development in more detail. Second, next to the scene network, other cortical category-specific high-level vision areas form networks. For example, face processing is supported by a core network with modules in the fusiform gyrus, inferior occipital gyrus, and superior temporal sulcus, for which evidence also suggests a prolonged functional development (e.g. Golarai et al., 2007; Nordt et al., 2018, for a review, see Haist and Anzures, 2017). Only little evidence, based on DTI analysis of major white matter tracts, exists that hints at possible emerging structure-function relations in the developing face processing system (Scherf et al., 2014). Using MWI and tractography of individual, short-range, face-area-specific tracts, future research might corroborate these first findings and shed more light on structural white matter development as a contributing developmental factor on the long way to (face) perception expertise.

## Author contributions

Conceptualization: TWM, SW; Methodology: EG, BM; Software: BM; Formal Analysis: TWM, EG; Investigation: TWM; Resources: SW, EG; Data Curation: TWM; Writing—Original Draft: TWM; Writing—Review and Editing: TWM, SW, EG, BM; Visualization: TWM; Supervision: SW, EG; Project Administration: TWM; Funding Acquisition: SW, TWM

## Acknowledgements

We thank our team of student assistants and interns for assisting in stimulus creation, pilot testing, subject recruiting, and data collection. We acknowledge the support of the Neuroimaging Centre of the Research Department of Neuroscience at Ruhr University Bochum's teaching hospital Bergmannsheil and Philips GmbH, Germany. We thank all participants and their parents for participating in this study.

## Funding

This work was supported by a PhD scholarship of the Konrad-Adenauer-Foundation and an International Realization Budget of the Ruhr University Bochum Research School PLUS through funds of the German Research Foundation's Universities Excellence Initiative (GSC 98/3) to TWM, grants from the German Research Foundation (GE 2777/2-1 and SFB 1280 project A03), the Mercator Research Center Ruhr (AN-2015-0044) to EG, and grants from the German Research Foundation (WE 5802/1-1 and SFB 1280 project A16), the Mercator Research Center Ruhr (AN-2014-0056), and the Volkswagen Foundation (Lichtenberg Professorship, 92 093) to SW.

## Data and code availability statement

All code used for data analysis (except for the MWF parameter map generating algorithm, which is available upon request), as well as anonymized raw data are publicly available at the Open Science Framework (https://osf.io/dbg83/, https://doi.org/10.17605/osf.io/dbg83).

## Ethics statement

The Ruhr University Bochum Faculty of Psychology ethics board approved the study (proposal no. 280). All participants as well as children's parents gave informed written consent to participate voluntarily.

## Conflict of interest statement

BM works at Philips GmbH, Hamburg, Germany. Philips is the manufacturer and support service provider for the MRI machine used in this study. BM developed and implemented the GRASE sequence at the scanner and co-developed and provided the MWF maps generating algorithm. BM and Philips GmbH had no role in the funding, conceptualization, design, or statistical analysis of the study.

# 5 References


Baldassano, C., Esteva, A., Fei-Fei, L., Beck, D.M., 2016. Two Distinct Scene-Processing Networks Connecting Vision and Memory. eNeuro 3 (5). 10.1523/ENEURO.0178-16.2016.

Barnea-Goraly, N., Menon, V., Eckert, M., Tamm, L., Bammer, R., Karchemskiy, A., Dant, C.C., Reiss, A.L., 2005. White matter development during childhood and adolescence: a cross-sectional diffusion tensor imaging study. Cereb Cortex 15 (12), 1848–1854. 10.1093/cercor/bhi062.

Behrens, T.E.J., Berg, H.J., Jbabdi, S., Rushworth, M.F.S., Woolrich, M.W., 2007. Probabilistic diffusion tractography with multiple fibre orientations: What can we gain? Neuroimage 34 (1), 144–155. 10.1016/j.neuroimage.2006.09.018.

Behrens, T.E.J., Woolrich, M.W., Jenkinson, M., Johansen-Berg, H., Nunes, R.G., Clare, S., Matthews, P.M., Brady, J.M., Smith, S.M., 2003. Characterization and propagation of uncertainty in diffusion-weighted MR imaging. Magn Reson Med 50 (5), 1077–1088. 10.1002/mrm.10609.

Bengtsson, S.L., Nagy, Z., Skare, S., Forsman, L., Forssberg, H., Ullén, F., 2005. Extensive piano practicing has regionally specific effects on white matter development. Nature neuroscience 8 (9), 1148–1150. 10.1038/nn1516.

Benner, T., van der Kouwe, A.J.W., Sorensen, A.G., 2011. Diffusion imaging with prospective motion correction and reacquisition. Magn Reson Med 66 (1), 154–167. 10.1002/mrm.22837.

Bettencourt, K.C., Xu, Y., 2013. The role of transverse occipital sulcus in scene perception and its relationship to object individuation in inferior intraparietal sulcus. J Cogn Neurosci 25 (10), 1711–1722. 10.1162/jocn_a_00422.

Carey, D., Caprini, F., Allen, M., Lutti, A., Weiskopf, N., Rees, G., Callaghan, M.F., Dick, F., 2018. Quantitative MRI provides markers of intra-, inter-regional, and age-related differences in young adult cortical microstructure. Neuroimage 182, 429–440. 10.1016/j.neuroimage.2017.11.066.

Chai, X.J., Ofen, N., Jacobs, L.F., Gabrieli, J.D.E., 2010. Scene complexity: Influence on perception, memory, and development in the medial temporal lobe. Front Hum Neurosci 4 (21), 21. 10.3389/fnhum.2010.00021.

Dale, A.M., Fischl, B., Sereno, M.I., 1999. Cortical surface-based analysis. I. Segmentation and surface reconstruction. Neuroimage 9 (2), 179–194. 10.1006/nimg.1998.0395.

Dean, D.C., O'Muircheartaigh, J., Dirks, H., Waskiewicz, N., Lehman, K., Walker, L., Han, M., Deoni, S.C.L., 2014. Modeling healthy male white matter and myelin development: 3 through 60months of age. Neuroimage 84, 742–752. 10.1016/j.neuroimage.2013.09.058.

Dean, D.C., O'Muircheartaigh, J., Dirks, H., Waskiewicz, N., Walker, L., Doernberg, E., Piryatinsky, I., Deoni, S.C.L., 2015. Characterizing longitudinal white matter development during early childhood. Brain Struct Funct 220 (4), 1921–1933. 10.1007/s00429-014-0763-3.

Deoni, S.C.L., Dean, D.C., O'Muircheartaigh, J., Dirks, H., Jerskey, B.A., 2012. Investigating white matter development in infancy and early childhood using myelin water faction and relaxation time mapping. Neuroimage 63 (3), 1038–1053. 10.1016/j.neuroimage.2012.07.037.

Deoni, S.C.L., Dean, D.C., Remer, J., Dirks, H., O'Muircheartaigh, J., 2015. Cortical maturation and myelination in healthy toddlers and young children. Neuroimage 115, 147–161. 10.1016/j.neuroimage.2015.04.058.

Deoni, S.C.L., Mercure, E., Blasi, A., Gasston, D., Thomson, A., Johnson, M., Williams, S.C.R., Murphy, D.G.M., 2011. Mapping infant brain myelination with magnetic resonance imaging. J Neurosci 31 (2), 784–791. 10.1523/JNEUROSCI.2106-10.2011.

Deoni, S.C.L., Rutt, B.K., Arun, T., Pierpaoli, C., Jones, D.K., 2008. Gleaning multicomponent T1 and T2 information from steady-state imaging data. Magn Reson Med 60 (6), 1372–1387. 10.1002/mrm.21704.

Dilks, D.D., Julian, J.B., Kubilius, J., Spelke, E.S., Kanwisher, N., 2011. Mirror-image sensitivity and invariance in object and scene processing pathways. J Neurosci 31 (31), 11305–11312. 10.1523/JNEUROSCI.1935-11.2011.

Epstein, R., Kanwisher, N., 1998. A cortical representation of the local visual environment. Nature 392 (6676), 598–601. 10.1038/33402.

Epstein, R.A., 2008. Parahippocampal and retrosplenial contributions to human spatial navigation. Trends Cogn Sci 12 (10), 388–396. 10.1016/j.tics.2008.07.004.

Epstein, R.A., Higgins, J.S., 2007. Differential parahippocampal and retrosplenial involvement in three types of visual scene recognition. Cereb Cortex 17 (7), 1680–1693. 10.1093/cercor/bhl079.

Epstein, R.A., Higgins, J.S., Jablonski, K., Feiler, A.M., 2007a. Visual scene processing in familiar and unfamiliar environments. J Neurophysiol 97 (5), 3670–3683. 10.1152/jn.00003.2007.

Epstein, R.A., Parker, W.E., Feiler, A.M., 2007b. Where am I now? Distinct roles for parahippocampal and retrosplenial cortices in place recognition. J Neurosci 27 (23), 6141–6149. 10.1523/JNEUROSCI.0799-07.2007.

Feldman, H.M., Yeatman, J.D., Lee, E.S., Barde, L.H.F., Gaman-Bean, S., 2010. Diffusion tensor imaging: a review for pediatric researchers and clinicians. J Dev Behav Pediatr 31 (4), 346–356. 10.1097/DBP.0b013e3181dcaa8b.

Fields, R.D., 2008. White matter in learning, cognition and psychiatric disorders. Trends Neurosci 31 (7), 361–370. 10.1016/j.tins.2008.04.001.

Fields, R.D., 2015. A new mechanism of nervous system plasticity: activity-dependent myelination. Nat Rev Neurosci 16 (12), 756–767. 10.1038/nrn4023.

Fischl, B., Rajendran, N., Busa, E., Augustinack, J., Hinds, O., Yeo, B.T.T., Mohlberg, H., Amunts, K., Zilles, K., 2008. Cortical folding patterns and predicting cytoarchitecture. Cereb Cortex 18 (8), 1973–1980. 10.1093/cercor/bhm225.

Fischl, B., Salat, D.H., Busa, E., Albert, M., Dieterich, M., Haselgrove, C., van der Kouwe, A., Killiany, R., Kennedy, D., Klaveness, S., Montillo, A., Makris, N., Rosen, B., Dale, A.M., 2002. Whole Brain Segmentation. Neuron 33 (3), 341–355. 10.1016/S0896-6273(02)00569-X.

Fischl, B., Sereno, M.I., Dale, A.M., 1999. Cortical surface-based analysis. II: Inflation, flattening, and a surface-based coordinate system. Neuroimage 9 (2), 195–207. 10.1006/nimg.1998.0396.

Fischl, B., van der Kouwe, A., Destrieux, C., Halgren, E., Ségonne, F., Salat, D.H., Busa, E., Seidman, L.J., Goldstein, J., Kennedy, D., Caviness, V., Makris, N., Rosen, B., Dale, A.M., 2004. Automatically parcellating the human cerebral cortex. Cereb Cortex 14 (1), 11–22.

Flechsig, P., 1920. Anatomie des menschlichen Gehirns und Rückenmarks auf myelogenetischer Grundlage. Thieme, Leipzig.

Ford, J.C., Hackney, D.B., Lavi, E., Phillips, M., Patel, U., 1998. Dependence of apparent diffusion coefficients on axonal spacing, membrane permeability, and diffusion time in spinal cord white matter. J Magn Reson Imaging 8 (4), 775–782. 10.1002/jmri.1880080405.

Geeraert, B.L., Lebel, R.M., Mah, A.C., Deoni, S.C., Alsop, D.C., Varma, G., Lebel, C., 2018. A comparison of inhomogeneous magnetization transfer, myelin volume fraction, and diffusion tensor imaging measures in healthy children. Neuroimage 182, 343–350. 10.1016/j.neuroimage.2017.09.019.

Genç, E., Bergmann, J., Singer, W., Kohler, A., 2011. Interhemispheric connections shape subjective experience of bistable motion. Curr Biol 21 (17), 1494–1499. 10.1016/j.cub.2011.08.003.

Golarai, G., Ghahremani, D.G., Whitfield-Gabrieli, S., Reiss, A., Eberhardt, J.L., Gabrieli, J.D.E., Grill-Spector, K., 2007. Differential development of high-level visual cortex correlates with category-specific recognition memory. Nat Neurosci 10 (4), 512–522. 10.1038/nn1865.

Gomez, J., Barnett, M.A., Natu, V., Mezer, A., Palomero-Gallagher, N., Weiner, K.S., Amunts, K., Zilles, K., Grill-Spector, K., 2017. Microstructural proliferation in human cortex is coupled with the development of face processing. Science 355 (6320), 68–71. 10.1126/science.aag0311.

Greve, D.N., Fischl, B., 2009. Accurate and robust brain image alignment using boundary-based registration. Neuroimage 48 (1), 63–72. 10.1016/j.neuroimage.2009.06.060.

Grill-Spector, K., 2003. The neural basis of object perception. Curr Opin Neurobiol 13 (2), 159–166. 10.1016/S0959-4388(03)00040-0.

Grydeland, H., Walhovd, K.B., Tamnes, C.K., Westlye, L.T., Fjell, A.M., 2013. Intracortical myelin links with performance variability across the human lifespan: results from T1- and T2-weighted MRI myelin mapping and diffusion tensor imaging. J Neurosci 33 (47), 18618–18630. 10.1523/JNEUROSCI.2811-13.2013.

Haist, F., Anzures, G., 2017. Functional development of the brain's face-processing system. Wiley Interdiscip Rev Cogn Sci 8 (1-2). 10.1002/wcs.1423.

Hasson, U., Harel, M., Levy, I., Malach, R., 2003. Large-Scale Mirror-Symmetry Organization of Human Occipito-Temporal Object Areas. Neuron 37 (6), 1027–1041. 10.1016/S0896-6273(03)00144-2.

Hodgetts, C.J., Shine, J.P., Lawrence, A.D., Downing, P.E., Graham, K.S., 2016. Evidencing a place for the hippocampus within the core scene processing network. Hum Brain Mapp 37 (11), 3779–3794. 10.1002/hbm.23275.

Hutchison, R.M., Culham, J.C., Everling, S., Flanagan, J.R., Gallivan, J.P., 2014. Distinct and distributed functional connectivity patterns across cortex reflect the domain-specific constraints of object, face, scene, body, and tool category-selective modules in the ventral visual pathway. Neuroimage 96, 216–236. 10.1016/j.neuroimage.2014.03.068.

Jenkinson, M., Bannister, P., Brady, M., Smith, S., 2002. Improved Optimization for the Robust and Accurate Linear Registration and Motion Correction of Brain Images. Neuroimage 17 (2), 825–841. 10.1006/nimg.2002.1132.

Jenkinson, M., Beckmann, C.F., Behrens, T.E.J., Woolrich, M.W., Smith, S.M., 2012. FSL. Neuroimage 62 (2), 782–790. 10.1016/j.neuroimage.2011.09.015.

Jenkinson, M., Smith, S., 2001. A global optimisation method for robust affine registration of brain images. Med Image Anal 5 (2), 143–156. 10.1016/S1361-8415(01)00036-6.

Jiang, P., Tokariev, M., Aronen, E.T., Salonen, O., Ma, Y., Vuontela, V., Carlson, S., 2014. Responsiveness and functional connectivity of the scene-sensitive retrosplenial complex in 7-11-year-old children. Brain Cogn 92C, 61–72. 10.1016/j.bandc.2014.10.005.

Jones, D.K., Knösche, T.R., Turner, R., 2013. White matter integrity, fiber count, and other fallacies: the do's and don'ts of diffusion MRI. Neuroimage 73, 239–254. 10.1016/j.neuroimage.2012.06.081.

Julian, J.B., Ryan, J., Hamilton, R.H., Epstein, R.A., 2016. The Occipital Place Area Is Causally Involved in Representing Environmental Boundaries during Navigation. Curr Biol 26 (8), 1104–1109. 10.1016/j.cub.2016.02.066.

Koldewyn, K., Yendiki, A., Weigelt, S., Gweon, H., Julian, J., Richardson, H., Malloy, C., Saxe, R., Fischl, B., Kanwisher, N., 2014. Differences in the right inferior longitudinal fasciculus but no general disruption of white matter tracts in children with autism spectrum disorder. Proc Natl Acad Sci USA 111 (5), 1981–1986. 10.1073/pnas.1324037111.

Laule, C., Kozlowski, P., Leung, E., Li, D.K.B., MacKay, A.L., Moore, G.R.W., 2008. Myelin water imaging of multiple sclerosis at 7 T: correlations with histopathology. Neuroimage 40 (4), 1575–1580. 10.1016/j.neuroimage.2007.12.008.

Laule, C., Leung, E., Lis, D.K.B., Traboulsee, A.L., Paty, D.W., MacKay, A.L., Moore, G.R.W., 2006. Myelin water imaging in multiple sclerosis: quantitative correlations with histopathology. Mult Scler 12 (6), 747–753. 10.1177/1352458506070928.

Lebel, C., Beaulieu, C., 2011. Longitudinal Development of Human Brain Wiring Continues from Childhood into Adulthood. J Neurosci 31 (30), 10937–10947. 10.1523/JNEUROSCI.5302-10.2011.

Loenneker, T., Klaver, P., Bucher, K., Lichtensteiger, J., Imfeld, A., Martin, E., 2011. Microstructural development: organizational differences of the fiber architecture between children and adults in dorsal and ventral visual streams. Hum Brain Mapp 32 (6), 935–946. 10.1002/hbm.21080.

MacKay, A., Whittall, K., Adler, J., Li, D., Paty, D., Graeb, D., 1994. In vivo visualization of myelin water in brain by magnetic resonance. Magn Reson Med 31 (6), 673–677.

McCarthy, P., 2018. FSLeyes. Zenodo. 10.5281/ZENODO.1470761.

Meissner, T.W., Genç, E., Mädler, B., Weigelt, S., 2019a. Myelination of major white matter tracts continues beyond childhood - combining tractography and myelin water imaging. bioRxiv. 10.1101/622233.

Meissner, T.W., Nordt, M., Weigelt, S., 2019b. Prolonged functional development of the parahippocampal place area and occipital place area. Neuroimage 191, 104–115. 10.1016/j.neuroimage.2019.02.025.

Meyers, S.M., Laule, C., Vavasour, I.M., Kolind, S.H., Mädler, B., Tam, R., Traboulsee, A.L., Lee, J., Li, D.K.B., MacKay, A.L., 2009. Reproducibility of myelin water fraction analysis: a comparison

of region of interest and voxel-based analysis methods. Magn Reson Imaging 27 (8), 1096–1103. 10.1016/j.mri.2009.02.001.

Miller, D.J., Duka, T., Stimpson, C.D., Schapiro, S.J., Baze, W.B., McArthur, M.J., Fobbs, A.J., Sousa, A.M.M., Sestan, N., Wildman, D.E., Lipovich, L., Kuzawa, C.W., Hof, P.R., Sherwood, C.C., 2012. Prolonged myelination in human neocortical evolution. Proc Natl Acad Sci USA 109 (41), 16480–16485. 10.1073/pnas.1117943109.

Miller, E.M., 1994. Intelligence and brain myelination: A hypothesis. Personality and Individual Differences 17 (6), 803–832. 10.1016/0191-8869(94)90049-3.

Moore, G.R.W., Leung, E., MacKay, A.L., Vavasour, I.M., Whittall, K.P., Cover, K.S., Li, D.K.B., Hashimoto, S.A., Oger, J., Sprinkle, T.J., Paty, D.W., 2000. A pathology-MRI study of the short-T2 component in formalin-fixed multiple sclerosis brain. Neurology 55 (10), 1506–1510. 10.1212/WNL.55.10.1506.

Moura, L.M., Kempton, M., Barker, G., Salum, G., Gadelha, A., Pan, P.M., Hoexter, M., Del Aquilla, M.A.G., Picon, F.A., Anés, M., Otaduy, M.C.G., Amaro, E., Rohde, L.A., McGuire, P., Bressan, R.A., Sato, J.R., Jackowski, A.P., 2016. Age-effects in white matter using associated diffusion tensor imaging and magnetization transfer ratio during late childhood and early adolescence. Magn Reson Imaging 34 (4), 529–534. 10.1016/j.mri.2015.12.021.

Mukherjee, P., Miller, J.H., Shimony, J.S., Conturo, T.E., Lee, B.C., Almli, C.R., McKinstry, R.C., 2001. Normal brain maturation during childhood: developmental trends characterized with diffusion-tensor MR imaging. Radiology 221 (2), 349–358. 10.1148/radiol.2212001702.

Nordt, M., Semmelmann, K., Genç, E., Weigelt, S., 2018. Age-related increase of image-invariance in the fusiform face area. Dev Cogn Neurosci 31, 46–57. 10.1016/j.dcn.2018.04.005.

O'Craven, K.M., Kanwisher, N., 2000. Mental imagery of faces and places activates corresponding stiimulus-specific brain regions. J Cogn Neurosci 12 (6), 1013–1023.

Oyefiade, A.A., Ameis, S., Lerch, J.P., Rockel, C., Szulc, K.U., Scantlebury, N., Decker, A., Jefferson, J., Spichak, S., Mabbott, D.J., 2018. Development of short-range white matter in healthy children and adolescents. Hum Brain Mapp 39 (1), 204–217. 10.1002/hbm.23836.

Prasloski, T., Rauscher, A., MacKay, A.L., Hodgson, M., Vavasour, I.M., Laule, C., Mädler, B., 2012. Rapid whole cerebrum myelin water imaging using a 3D GRASE sequence. Neuroimage 63 (1), 533–539. 10.1016/j.neuroimage.2012.06.064.

Pruessmann, K.P., Weiger, M., Scheidegger, M.B., Boesiger, P., 1999. SENSE: Sensitivity encoding for fast MRI. Magn Reson Med 42 (5), 952–962. 10.1002/(SICI)1522-2594(199911)42:5<952:AID-MRM16>3.3.CO;2-J.

Pujol, J., Soriano-Mas, C., Ortiz, H., Sebastián-Gallés, N., Losilla, J.M., Deus, J., 2006. Myelination of language-related areas in the developing brain. Neurology 66 (3), 339–343. 10.1212/01.wnl.0000201049.66073.8d.

R Core Team, 2015. R: A Language and Environment for Statistical Computing, Vienna, Austria. http://www.R-project.org/.

Rollins, N.K., Glasier, P., Seo, Y., Morriss, M.C., Chia, J., Wang, Z., 2010. Age-related variations in white matter anisotropy in school-age children. Pediatr Radiol 40 (12), 1918–1930. 10.1007/s00247-010-1744-1.

Scherf, K.S., Thomas, C., Doyle, J., Behrmann, M., 2014. Emerging structure-function relations in the developing face processing system. Cereb Cortex 24 (11), 2964–2980. 10.1093/cercor/bht152.

Ségonne, F., Dale, A.M., Busa, E., Glessner, M., Salat, D., Hahn, H.K., Fischl, B., 2004. A hybrid approach to the skull stripping problem in MRI. Neuroimage 22 (3), 1060–1075. 10.1016/j.neuroimage.2004.03.032.

Shafee, R., Buckner, R.L., Fischl, B., 2015. Gray matter myelination of 1555 human brains using partial volume corrected MRI images. Neuroimage 105, 473–485. 10.1016/j.neuroimage.2014.10.054.

Smith, S.M., 2002. Fast robust automated brain extraction. Hum Brain Mapp 17 (3), 143–155. 10.1002/hbm.10062.

Takahashi, M., Hackney, D.B., Zhang, G., Wehrli, S.L., Wright, A.C., O'Brien, W.T., Uematsu, H., Wehrli, F.W., Selzer, M.E., 2002. Magnetic resonance microimaging of intraaxonal water

diffusion in live excised lamprey spinal cord. Proc Natl Acad Sci USA 99 (25), 16192–16196. 10.1073/pnas.252249999.

van Wedeen, J., Hagmann, P., Tseng, W.-Y.I., Reese, T.G., Weisskoff, R.M., 2005. Mapping complex tissue architecture with diffusion spectrum magnetic resonance imaging. Magn Reson Med 54 (6), 1377–1386. 10.1002/mrm.20642.

Vass, L.K., Epstein, R.A., 2013. Abstract representations of location and facing direction in the human brain. J Neurosci 33 (14), 6133–6142. 10.1523/JNEUROSCI.3873-12.2013.

Woolrich, M.W., Behrens, T.E.J., Beckmann, C.F., Jenkinson, M., Smith, S.M., 2004. Multilevel linear modelling for FMRI group analysis using Bayesian inference. Neuroimage 21 (4), 1732–1747. 10.1016/j.neuroimage.2003.12.023.

Woolrich, M.W., Ripley, B.D., Brady, M., Smith, S.M., 2001. Temporal autocorrelation in univariate linear modeling of FMRI data. Neuroimage 14 (6), 1370–1386. 10.1006/nimg.2001.0931.

Yakovlev, P.I., Lecours, A.-R., 1967. The myelogenetic cycles of regional maturation of the brain, in: Minkowski, A. (Ed.), Regional Development of the Brain Early in Life. Blackwell Scientific Publications Inc., Boston, MA, pp. 3–70.

Yeatman, J.D., Dougherty, R.F., Ben-Shachar, M., Wandell, B.A., 2012. Development of white matter and reading skills. Proc Natl Acad Sci USA 109 (44), E3045-53. 10.1073/pnas.1206792109.

Yendiki, A., Panneck, P., Srinivasan, P., Stevens, A., Zöllei, L., Augustinack, J., Wang, R., Salat, D., Ehrlich, S., Behrens, T., Jbabdi, S., Gollub, R., Fischl, B., 2011. Automated probabilistic reconstruction of white-matter pathways in health and disease using an atlas of the underlying anatomy. Front Neuroinform 5, 23. 10.3389/fninf.2011.00023.

Zatorre, R.J., Fields, R.D., Johansen-Berg, H., 2012. Plasticity in gray and white: neuroimaging changes in brain structure during learning. Nat Neurosci 15 (4), 528–536. 10.1038/nn.3045.